

ANGULAR AND ENERGY DISTRIBUTIONS OF PHOTONEUTRONS FROM BISMUTH,
GOLD, AND TANTALUM

G. N. ZATSEPINA, V. V. IGONIN, L. E. LAZAREVA, and A. I. LEPESTKIN

P. N. Lebedev Physics Institute, Academy of Sciences, U.S.S.R.

Submitted to JETP editor January 2, 1963

J. Exptl. Theoret. Phys. (U.S.S.R.) 44, 1787-1799 (June, 1963)

Results are reported of measurements of the angular and energy distributions of photoneutrons from bismuth, gold, and tantalum irradiated by x rays of 14 and 19 MeV peak energy. The results are analyzed from the standpoint of the independent particle model.

OWING to the high Coulomb barrier, the photo-disintegration of heavy nuclei can be accompanied by the emission of protons and other charged particles at gamma-quantum energies higher than the giant-resonance region. An investigation of the interaction between gamma quanta and nuclei in the giant resonance region is possible in this case only with the aid of photoneutrons. In this connection, the study of the angular and energy distributions of photoneutrons from heavy nuclei at low excitation energies is of appreciable interest.

We present the results of measurements of the angular and energy distributions of photoneutrons from specimens of bismuth, gold, and tantalum irradiated by gamma bremsstrahlung with maximum energy $(h\nu)_{\max}$ 14 and 19 MeV. The work was done with the 30-MeV synchrotron of the Academy of Sciences Physics Institute.

1. OBSERVATION PROCEDURE

The spectra of the photoneutrons emitted at different angles (ϑ) to the x-ray beam direction, were measured by registering the recoil protons in nuclear emulsions. Figure 1 shows the arrangement of the specimen and of the emulsions during the irradiation.

The specimens were in the forms of discs 40 mm in diameter. The bismuth, gold, and tantalum were 3.91, 3.77, and 3.41 g/cm² thick, respectively. In measurements of the background, the investigated specimen was replaced by a graphite disc of the same diameter 0.93 g/cm² thick. The thicknesses of the specimens and of the graphite disc were chosen such that the neutrons present in the x-ray beam were always scattered by approximately the same amount ($\approx 7\%$). No photoneutrons are emitted from graphite up to a gamma-ray energy ~ 19 MeV (the threshold energy of the reac-

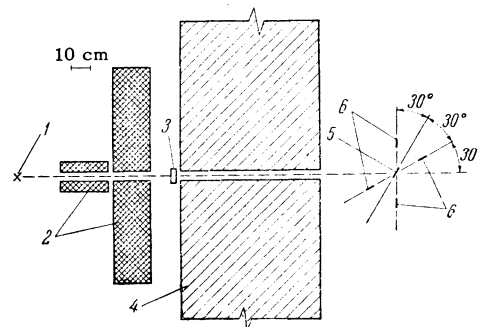


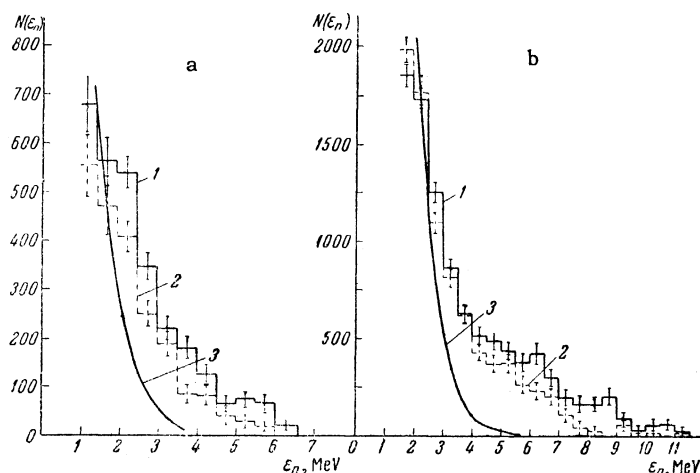
FIG. 1. Placement of the specimen and emulsions during the irradiation: 1 - synchrotron target, 2 - lead collimator, 3 - thin-wall ionization chamber and integrator, 4 - paraffin wall, 5 - specimen, 6 - emulsions.

tion $C^{12}(\gamma, n)$ is 18.7 MeV), so that such background determination is most accurate up to this energy. The radiation dose was measured with a thin-wall integral ionization chamber placed in the x-ray beam behind the collimator.

Type NIKFI Ya-2 emulsions 400 μ thick and measuring 3 by 5 cm were located 16 cm from the center of the specimens, at angles ϑ equal to 30, 90, 150, and 270°. It is seen from Fig. 1 that at the chosen relative placement of the specimen and emulsions, the solid angles were the same for all emulsions. The error in the determination of the direction of motion of the neutrons, due to the finite dimensions of the specimen and of the plates, amounted on the average to 3°.

The emulsions were scanned with MBI-2 microscopes with 60 \times objectives and 5 \times eyepieces. When measuring the track parameters, the 5 \times eyepiece was replaced by a 10 \times one. Only recoil protons scattered at small angles relative to the direction of neutron motion were registered, namely $\pm 15^\circ$ in the plane of the emulsion and $\pm 20^\circ$ in the depth of the emulsions. The scattering angles were

FIG. 2. Energy distributions of photoneutrons from bismuth irradiated by x-rays with maximum energy $(h\nu)_{\max} = 14$ MeV (a) and 19 MeV (b) for different emission angles: histogram 1— $N_{90^\circ} + N_{270^\circ}$, histogram 2— $N_{30^\circ} + N_{150^\circ}$. Curve 3—neutron spectrum calculated in accordance with the evaporation model.



measured and taken into account in the calculations of the neutron energies. The obtained neutron spectrum was corrected for the variation of the np scattering cross section with the energy and for the missing tracks leaving the emulsion.

Since the number of missed tracks is relatively large at low energies, the obtained energy distributions are given starting from 1 MeV for $(h\nu)_{\max} = 14$ MeV (since the spectrum is softer in this case, the scanning has been carried out more meticulously), and starting with 1.5 MeV for $(h\nu)_{\max} = 19$ MeV. Since the scatter of the data exceeded in the first energy interval the statistical value (owing to fluctuations in the missed tracks and to the relatively high background), this interval is not used in the discussion of the results. For $(h\nu)_{\max} = 14$ MeV with neutrons of energy $\epsilon_n \geq 1.5$ MeV the background was approximately 2% for $\vartheta = 90^\circ$ and approximately 14% for $\vartheta = 30^\circ$. For $(h\nu)_{\max} = 19$ MeV with neutrons of energy $\epsilon_n \geq 2$ MeV the background was $\sim 1.5\%$ for $\vartheta = 90^\circ$ and approximately 10% for $\vartheta = 30^\circ$.

2. MEASUREMENT RESULTS AND DISCUSSION

Bismuth. Figure 2 shows the energy spectra of photoneutrons from bismuth, obtained for the two maximum x-ray energies 14 and 19 MeV. Histogram 1 is the energy distribution of the neutrons emitted at right angles to the x-ray beam direction, i.e., the value of $N_{90^\circ} + N_{270^\circ}$. Histogram 2 gives the summary neutron spectrum for angles $\vartheta = 30^\circ$ and 150° ($N_{30^\circ} + N_{150^\circ}$)¹⁾. Both distributions pertain to equal scanned emulsion area.

¹⁾The present measurement accuracy is insufficient for the analysis of the difference in the yield of the more energetic neutrons for angles ϑ equal to 30° and 150° , observed with threshold detectors^[1].

Together with the experimental data, the figure shows for each irradiation energy also the neutron spectra calculated for the evaporation model (curve 3). The calculation was made for a level density^[2].

$$\omega = C \exp [3.35 (A - 40)^{1/2} (E - E_0 - \epsilon_n)]^{1/2}$$

(C is a constant, A the mass number, E the nuclear excitation energy, E_0 the neutron binding energy, and ϵ_n the energy of the emitted neutron). The cross sections of the (γ, n) and $(\gamma, 2n)$ reactions were taken from the paper of Gavrilov and Lazareva^[3]. The Schiff spectrum was assumed for the x-rays^[4]. Curves 3 are coincident in the low-energy region with the experimental distributions ($N_{30^\circ} + N_{150^\circ}$), where the relative fraction of the neutrons emitted as a result of the evaporation should be the largest.²⁾

The sharp difference between the experimental spectra and the spectrum calculated by the evaporation model, observed for $(h\nu)_{\max} = 19$ MeV, agrees with the results of several investigations made on bismuth at x-ray energies $(h\nu)_{\max}$ from 19 to 30 MeV^[5]. It is interesting that the same sharp difference is observed for $(h\nu)_{\max} = 14$ MeV. This means that at gamma-quantum energies below the maximum of giant resonance, as well as at larger energies, a considerable part of the neutrons is emitted as a result of the direct interaction between the gamma quanta and the individual nucleons of the nucleus.

As can be seen from Fig. 2, the distributions $N_{90^\circ} + N_{270^\circ}$ and $N_{30^\circ} + N_{150^\circ}$ differ rather strongly from each other, owing to the anisotropic part of the "direct" photoneutrons. Table I lists the

²⁾The first energy interval on histogram 2 was not used to normalize curve 3, since the neutron yields obtained in this interval could be somewhat undervalued.

Table I

$(h\nu)_{\max} = 14$ MeV		$(h\nu)_{\max} = 19$ MeV	
Intervals of ϵ_n , MeV	$(N_{90^\circ} + N_{270^\circ})$	Intervals of ϵ_n , MeV	$(N_{90^\circ} + N_{270^\circ})$
	$(N_{30^\circ} + N_{150^\circ})$		$(N_{30^\circ} + N_{150^\circ})$
1.5÷3	1.28±0.11	1.5÷2.5	0.96±0.03
2÷3	1.35±0.12	2.5÷4	1.08±0.05
3÷6,6	1.67±0.22	4÷5.5	1.23±0.11
4÷6,6	2.30±0.57	5,5÷7	1.59±0.22
		5÷11.5	2.12±0.25

ratios $\eta = (N_{90^\circ} + N_{270^\circ}) / (N_{30^\circ} + N_{150^\circ})$ for different intervals of the energy ϵ_n . Both for $(h\nu)_{\max} = 14$ MeV and for $(h\nu)_{\max} = 19$ MeV the anisotropy increases with increasing photoneutron energy. If the angular distribution is described in general form by the expression $I(\vartheta) = a + b \sin^2 \vartheta + A \cos \vartheta + B \sin^2 \vartheta \cos \vartheta$ [6], then upon summation of $I(\vartheta)$ and $I(\pi - \vartheta)$ the terms that produce an asymmetric shift forward drop out and $I(\vartheta) + I(\pi - \vartheta) \sim a + b \sin^2 \vartheta$. The ratio η listed in Table I is equal to $(1 + b/a)(1 + b/4a)$. For $(h\nu)_{\max} = 14$ MeV in the interval 3.5–6.6 MeV, in which there are practically no evaporation nuclei, we have $\eta = 1.7 - 1.8$. This corresponds to $b/a = 1.2$ to 1.45 . For $(h\nu)_{\max} = 19$ MeV one can see particularly clearly the increase in the ratio η towards the end of the spectrum, as the fraction of the direct neutrons increases. In the interval from 5.5 to 11.5 MeV this ratio amounts to approximately 1.8 (above ~ 7 MeV the errors become too large, so that the further increase in η observed for the very end of the spectrum cannot be ascribed any significance). This yields $b/a \sim 1.4$.

Table II lists the levels of Bi^{209} , for which the neutron binding energies are lower than 19 MeV. The binding energies (second column) are taken from the nuclide energy level scheme calculated by Ross, Mark, and Lawson [7] for a diffuse nuclear potential. In the third column of the table are calculated the possible dipole transitions to the corresponding excited single-particle levels. For other dipole transitions, either the shell to which the nucleon should go is completely filled (in this case this occurs for all transitions of type $nl \rightarrow nl - 1$), or the sum of the spin and orbital momenta changes by two, or else the overlap integral is very small.

Figure 3 shows the relative yields of the "direct" neutrons from individual shells of Bi^{209} irradiated with x-rays having $(h\nu)_{\max}$ equal to 14 and 19 MeV, calculated by the Wilkinson independent-particle model [8]. It was assumed in the calculation that all the E1 transitions listed in Table II can occur (the energies of the corresponding excited single-particle states are posi-

Table II

Neutron levels	Binding energy, MeV	Possible dipole transitions	Relative intensities of transitions
$3p^{1/2}$	7.7	$3p^{1/2} \rightarrow 3d^{3/2}$ $(nl - 1/2 \rightarrow nl + 1 - 1/2)$	0.17
$3p^{3/2}$	8.4	$3p^{1/2} \rightarrow 3d^{5/2}$ $(nl + 1/2 \rightarrow nl + 1 + 1/2)$ $3p^{3/2} \rightarrow 3d^{3/2}$ $(nl + 1/2 \rightarrow nl + 1 - 1/2)$	0.30 0.03
$2f^{5/2}$	8.8	$2f^{3/2} \rightarrow 2g^{7/2}$ $(nl - 1/2 \rightarrow nl + 1 - 1/2)$	0.63
$1i^{3/2}$	10.1	$1i^{3/2} \rightarrow 1f^{5/2}$ $(nl + 1/2 \rightarrow nl + 1 + 1/2)$ $1i^{3/2} \rightarrow 1f^{3/2}$ $(nl + 1/2 \rightarrow nl + 1 - 1/2)$	2.16 0.02
$2f^{7/2}$	10.8	$2f^{7/2} \rightarrow 2g^{9/2}$ $(nl + 1/2 \rightarrow nl + 1 + 1/2)$ $2f^{7/2} \rightarrow 2g^{7/2}$ $(nl + 1/2 \rightarrow nl + 1 - 1/2)$	0.82 0.02
$1h^{3/2}$	13.1	$1h^{3/2} \rightarrow 1i^{11/2}$ $(nl - 1/2 \rightarrow nl + 1 - 1/2)$ $1h^{3/2} \rightarrow 2g^{9/2}$ $(nl - 1/2 \rightarrow (n + 1)l - 1 + 1/2)$ $1h^{3/2} \rightarrow 2g^{7/2}$ $(nl - 1/2 \rightarrow (n + 1)l - 1 - 1/2)$	1.53 0.002 0.08

tive). The relative intensities of these transitions, taken from the tables given by Wilkinson [8], are listed in the fourth column of Table II.

The relative probabilities of the "direct" photoeffect were calculated, following Wilkinson [8], using the formula

$$C = kP\hbar^2/WMR,$$

where k is the wave number of the emitted nucleon, P the centrifugal barrier penetrance coefficient, \hbar Planck's constant, M the nucleon mass, R the nuclear radius³⁾ and W the imaginary part of the

³⁾We used $R = 1.3 \times 10^{-13} A^{1/3}$ in the calculations.

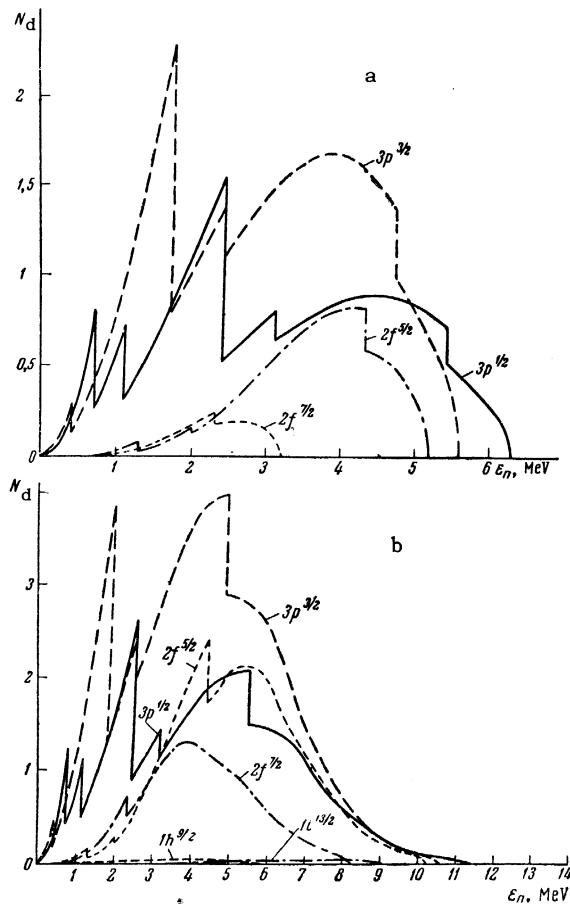


FIG. 3. Relative yields of "direct" neutrons from individual shells of Bi^{209} irradiated by x-rays with $(h\nu)_{\text{max}} = 14$ MeV (a) and 19 MeV (b), calculated in accordance with the independent-particle model.

optical potential. The penetrances of the centrifugal barrier for neutrons with different values of l were calculated with formula (5.7) of the book of Blatt and Weisskopf^[9] (the values of the functions v_l and v_l' were taken from the tables of Lax and Feshbach^[10]). The values used for W were obtained from a detailed analysis of all the available experimental data for neutrons, carried out by Nemirovskii. These values vary linearly with the neutron energy from 2.5 MeV at $\epsilon_n = 0$ to 8 MeV at $\epsilon_n = 14$ MeV. The cross sections for nuclear absorption and the x-ray spectra were taken from Gavrilov and Lazareva^[3] and Schiff^[4].

The kinks in the spectra of the "direct" neutrons, shown in Fig. 3, correspond to γ -quantum energies at which neutron emission is possible from a new level (equal to the binding energies for this level). The addition of a new excitation channel under the condition of slow variation of the absorption cross section sharply reduces the relative probabilities of the other transitions, and consequently also the yields of the "direct" neu-

trons from the other shells. If the absorption cross section curves actually have narrow peaks at these energies, there should be no such kinks.

The summary spectrum of the "direct" neutrons has a broad maximum. Its position ($\epsilon_n \sim 3.5$ MeV at $(h\nu)_{\text{max}} = 14$ MeV, $\epsilon_n \sim 5$ MeV at $(h\nu)_{\text{max}} = 19$ MeV) corresponds to the maximum in the distribution of the effective quanta, i.e., to the maximum of $\sigma_{\text{abs}}(h\nu)n(h\nu, h\nu_{\text{max}})$, where σ_{abs} is the cross section for nuclear absorption of the γ quanta and $n(h\nu, h\nu_{\text{max}})$ is the number of quanta of given energy at a maximum x-ray energy equal to $(h\nu)_{\text{max}}$.

As can be seen from Fig. 3, the main transitions in the direct emission of photoneutrons are the transitions from the p- and f-shells. Owing to the large values of the energy and the large values of l , the levels $1i^{13/2}$ and $1h^{9/2}$ practically do not participate in the direct photoeffect.

The angular distributions in the transitions $l \rightarrow l + 1$ from the p- and f-shells should have respectively the form^[12] $1 + 1.5 \sin^2 \vartheta$ and $1 + 0.8 \times \sin^2 \vartheta$. The fact that for both values of $(h\nu)_{\text{max}}$ (14 and 19 MeV) the experimental values of the ratio b/a for the neutrons with higher energy are close to 1.5 indicates that for this part of the spectrum of the "direct" neutrons the main transitions are those from the p-shells. This agrees with the general picture obtained by calculation for the direct-interaction process (Fig. 3).

Wataghin et al.^[5], who measured the angular and energy distributions of photoneutrons from bismuth at $(h\nu)_{\text{max}} = 22$ MeV, found that the ratio b/a as a function of the neutron energy has a maximum at $\epsilon_n = 5.5$ MeV. In view of the analysis made and in view of the low accuracy of their data for the end of the spectrum this conclusion is doubtful.

If the angular distribution is described with sufficient accuracy by the expression $a + b \sin^2 \vartheta$, then the sum of the obtained distributions $(N_{90^\circ} + N_{270^\circ}) + (N_{30^\circ} + N_{150^\circ})$ should correspond approximately in form to an integral neutron spectrum $N(\epsilon_n) \sim a + 2b/3$.

Figure 4 shows (histogram 1) the summary energy distribution of the photoneutrons for 30, 90, 150, and 270° at $(h\nu)_{\text{max}} = 19$ MeV. The same figure shows the calculated spectrum of the "direct" neutrons, $N_d(\epsilon_n)$, which is the sum of the curves shown in Fig. 3. The theoretical curve 2 is made coincident with the experimental distribution in the energy region $\epsilon_n > 5$ MeV, where there are practically no evaporation neutrons. In this part of the spectrum the histogram 1 and curve 2 are in remarkably good agreement.

The dashed lines (histogram 3) show the yields of the evaporation neutrons $N_{Ev}(\epsilon_n)$, obtained by subtracting from the experimental distribution 1 the calculated spectrum 2 of the "direct" neutrons. Histogram 3 is in very good agreement with the neutron spectrum 4 calculated from the evaporation model (they are coincident in the interval $\epsilon_n = 2-2.5$ MeV). This means that in the energy region $\epsilon_n < 5$ MeV, where the evaporation process predominates, the calculated spectrum of the "direct" neutrons is also in sufficiently good agreement with the true spectrum. The ratio of the areas under curves 2 and 4 (the total area is taken for curve 4, starting with $\epsilon_n = 0$) yields $N_d/N_{Ev} = 17\%$. In the case when $(h\nu)_{max} = 14$ MeV the theoretical and experimental curves also agree in general outline. However, owing to the large experimental errors this agreement is somewhat worse. The ratio N_d/N_{Ev} is found to be 15–20% for $(h\nu)_{max} = 14$ MeV.

Gold. Figure 5 shows the spectra of the photoneutrons obtained by irradiating gold with x-rays having $(h\nu)_{max} = 14$ MeV. Histograms 1 and 2 represent the neutron spectra for 90 and 270° ($N_{90^\circ} + N_{270^\circ}$) and for 30 and 150° ($N_{30^\circ} + N_{150^\circ}$), respectively, referred to equal emulsion area.

In this case no sharp angular anisotropy is observed in the neutron yield. The energy distributions $N_{90^\circ} + N_{270^\circ}$ and $N_{30^\circ} + N_{150^\circ}$ differ less from the distribution calculated in analogy with bismuth for the evaporation process (curve 3). This is seen particularly clearly from the comparison of the spectra of the neutrons from bismuth and from gold, shown in Fig. 6⁴).

The sharper decrease in neutron yield with increasing energy ϵ_n , observed for gold, was also obtained for an angle $\vartheta = 90^\circ$ by Bertozzi, Paolini, and Sargent^[13], who measured the spectrum of photoneutrons from bismuth and gold irradiated by x-rays with $(h\nu)_{max} = 14.3$ MeV by the time of flight method. The $\ln[N(\epsilon_n)/\epsilon_n]$ curves obtained by them have sharply pronounced slopes at the end of the spectrum, with the curve for gold being much steeper. Starting from the data shown in Fig. 6, the interval yield of the "direct" neutrons with energy $\epsilon_n > 3$ MeV is approximately 1.5 times less from gold than from bismuth.

Everything said with regard to the distribution obtained for $(h\nu)_{max} = 14$ MeV can be repeated for $(h\nu)_{max} = 19$ MeV (for which the data are omitted so as not to overburden the article with too many figures).

⁴To make the irradiation and scanning conditions more identical, we chose for bismuth only those irradiation series in which gold was also irradiated.

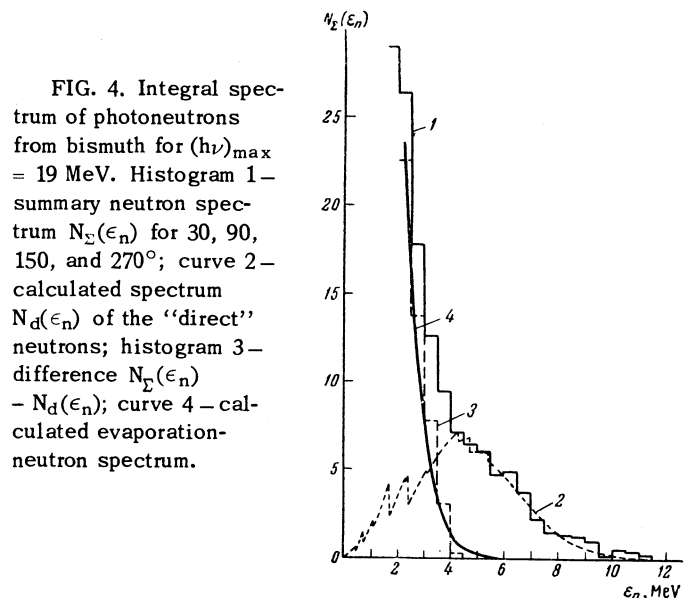


FIG. 4. Integral spectrum of photoneutrons from bismuth for $(h\nu)_{max} = 19$ MeV. Histogram 1—summary neutron spectrum $N_{\Sigma}(\epsilon_n)$ for 30, 90, 150, and 270°; curve 2—calculated spectrum $N_d(\epsilon_n)$ of the "direct" neutrons; histogram 3—difference $N_{\Sigma}(\epsilon_n) - N_d(\epsilon_n)$; curve 4—calculated evaporation-neutron spectrum.

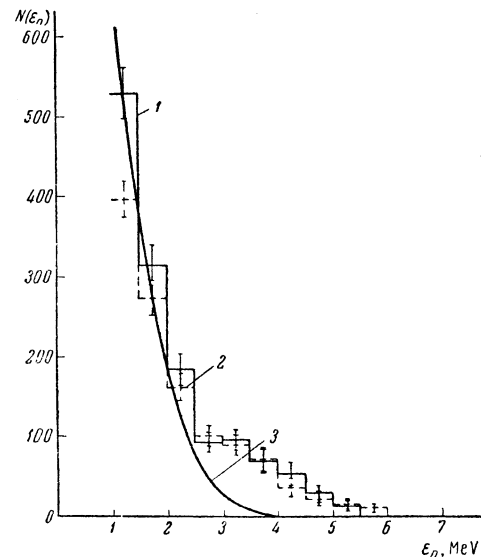


FIG. 5. Energy distribution of photoneutrons from gold at $(h\nu)_{max} = 14$ MeV; histogram 1— $N_{90^\circ} + N_{270^\circ}$; histogram 2— $N_{30^\circ} + N_{150^\circ}$; curve 3—neutron spectrum calculated in accordance with the evaporation model.

Table III lists the neutron levels capable of participating in the E1 transitions when gold is excited with gamma rays of energy up to 19 MeV. The level scheme and the binding energies are also taken from the paper of Ross et al.^[7]

Figure 7 shows the spectra of the "direct" neutrons from the individual shells, calculated as for bismuth by the independent-particle model. From the given level scheme it follows that when $(h\nu)_{max} = 14$ MeV the neutrons with energy higher than 3.5 MeV should be emitted in practice only from the $3p^{3/2}$ shell. The lack of noticeable experimentally observed angular anisotropy, on the other hand, indicates that the $3p^{3/2} \rightarrow 3d^{5/2}$ transitions should

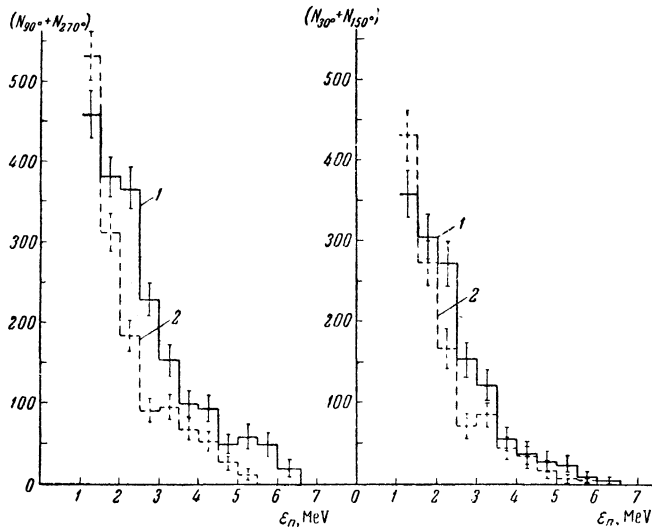


FIG. 6. Comparison of the spectra of photoneutrons from bismuth (1) and gold (2) for different emission angles at $(h\nu)_{\max} = 14$ MeV.

Table III

Neutron levels	Binding energy, MeV	Possible dipole transitions	Relative intensities of transitions
$3p^{3/2}$	8.0	$3p^{3/2} \rightarrow 3d^{3/2}$	0.30
		$(nl + 1/2 \rightarrow nl + 1 + 1/2)$	0.03
		$3p^{3/2} \rightarrow 3d^{5/2}$	0.03
$1i^{13/2}$	8.9	$(nl + 1/2 \rightarrow nl + 1 - 1/2)$	2.16
		$1i^{13/2} \rightarrow 1j^{13/2}$	0.02
		$(nl + 1/2 \rightarrow nl + 1 + 1/2)$	0.02
$1h^{9/2}$	10.3	$1h^{9/2} \rightarrow 1i^{11/2}$	1.53
		$(nl - 1/2 \rightarrow nl + 1 - 1/2)$	0.002
		$1h^{9/2} \rightarrow 2g^{7/2}$	0.08
$2f^{7/2}$	10.5	$(nl - 1/2 \rightarrow (n + 1)l - 1 + 1/2)$	0.82
		$1h^{9/2} \rightarrow 2g^{7/2}$	0.02
		$(nl + 1/2 \rightarrow nl + 1 - 1/2)$	0.02
$3s^{1/2}$	14.7	$3s^{1/2} \rightarrow 3p^{1/2}$	0.07
		$(nl + 1/2 \rightarrow nl + 1 - 1/2)$	0.07
$2d^{3/2}$	15.0	$2d^{3/2} \rightarrow 2f^{5/2}$	0.40
		$(nl - 1/2 \rightarrow nl + 1 - 1/2)$	0.06
$1h^{11/2}$	15.2	$2d^{3/2} \rightarrow 3p^{1/2}$	0.06
		$(nl - 1/2 \rightarrow (n + 1)l - 1 - 1/2)$	0.02
$2d^{5/2}$	16.8	$1h^{11/2} \rightarrow 1i^{11/2}$	0.02
		$(nl + 1/2 \rightarrow nl + 1 - 1/2)$	0.10
$1g^{7/2}$	17.6	$1h^{11/2} \rightarrow 2d^{9/2}$	0.10
		$(nl + 1/2 \rightarrow (n + 1)l - 1 + 1/2)$	0.03
		$2d^{5/2} \rightarrow 2f^{5/2}$	0.03
		$(nl + 1/2 \rightarrow nl + 1 - 1/2)$	0.03
		$1g^{7/2} \rightarrow 2f^{5/2}$	0.07
		$(nl - 1/2 \rightarrow (n + 1)l - 1 - 1/2)$	0.07

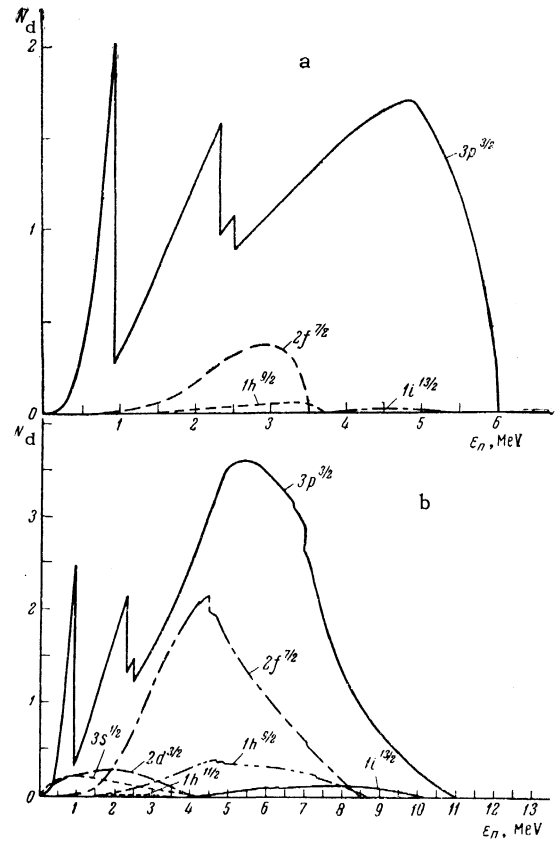


FIG. 7. Relative yields of "direct" neutrons from individual shells of the Au^{197} nucleus irradiated by x-rays with $(h\nu)_{\max} = 14$ MeV (a) and 19 MeV (b), calculated in accordance with the independent particle model.

not play a noticeable role in the direct emission of the photoneutrons.

Figure 8 shows the summary neutron spectra $N_{30^\circ} + N_{90^\circ} + N_{150^\circ} + N_{270^\circ}$ for gold with $(h\nu)_{\max} = 14$ and 19 MeV. The same figure shows the spectra of the "direct" neutrons obtained by adding up the curves calculated for the individual shells (see Fig. 7).

In the case $(h\nu)_{\max} = 14$ MeV the forms of the calculated and experimental spectra differ strongly in the energy region $\epsilon_n > 3.5$ MeV. All this indicates that the $3p^{3/2} \rightarrow 3d^{5/2}$ transitions do not participate noticeably in the direct neutron emission. It must be noted that the level scheme obtained for gold in [7] does not agree with the scheme of filled levels given for Au^{197} by Goepfert-Mayer and Jensen [14]. According to the latter, the $3p^{3/2}$ level is free, but the $2f^{5/2}$ level is filled. Unfortunately, there are no reliable data at present to permit a rigorous analysis in accord with the independent particle model.

In the case $(h\nu)_{\max} = 19$ MeV in the energy region $\epsilon_n > 5$ MeV the neutrons can be emitted from the $2f^{7/2}$ shell in addition to the $3p^{3/2}$ shell. The fact that the calculated spectrum of the "direct"

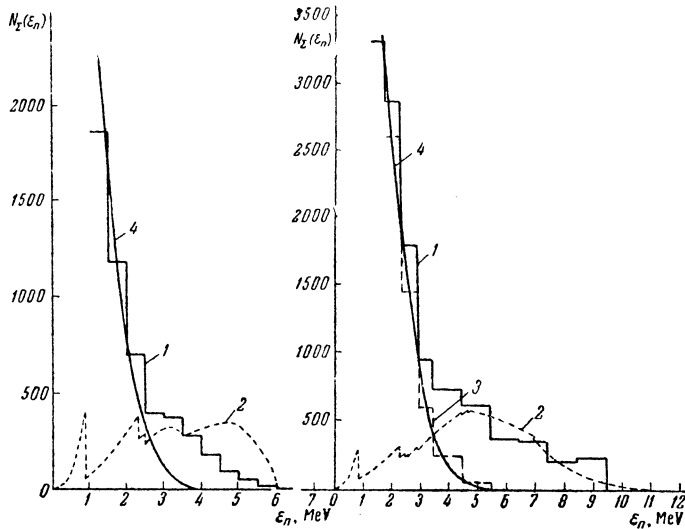


FIG. 8. Integral spectra of photoneutrons from gold at $(h\nu)_{\max} = 14$ MeV (a) and 19 MeV (b); histogram 1 – summary neutron spectrum $N_{\Sigma}(\epsilon_n)$ for 30, 90, 150, and 270°; curve 2 – calculated spectrum $N_d(\epsilon_n)$ of the “direct” neutrons; histogram 3 – difference $N_{\Sigma}(\epsilon_n) - N_d(\epsilon_n)$; curve 4 – calculated spectrum of evaporation neutrons.

neutrons and the experimental spectrum of the neutrons agree in general outline in this energy region, can obviously be attributed to the approximate similarity of the curves for the p- and f-shells in Fig. 6. An estimate of the fraction of the “direct” neutrons, similar to that for bismuth, yields for gold $N_d/N_{\text{ev}} \sim 12\%$.

The calculation made in the present work by the Wilkinson independent-particle model for bismuth and gold gives the following “direct” neutron yields as fractions of the total number of emitted neutrons:

$(h\nu)_{\max}$, MeV:	14	19
Yield for Bi, %:	6.0	7.0
Yield for Au, %:	3.2	4.7

No account was taken in the calculations of the fact that protons can also go over to the single-particle excited levels upon absorption of the gamma quanta. In view of the high Coulomb barrier, practically all these cases will lead to the formation of a com-

pound nucleus with subsequent evaporation. Thus, the yields presented should be somewhat too high.

The ratio of the yields from bismuth and gold, obtained by experiment, agrees with the calculations. The ratios N_d/N_{tot} presented above are 3–4 times smaller than the calculated ones in absolute magnitude. The calculated and experimental data can apparently be reconciled by using in the calculations of the probability of direct emission $C = kPk^2/WMR$ (see above) somewhat different values for R and W, and perhaps also P.

Tantalum. The spectrum of the photoneutrons from tantalum was measured only for x-rays with maximum energy of 19 MeV. Figure 9a shows the energy distributions for 90 and 270° and for 30 and 150°. As in the case of bismuth and gold, there was no sense in comparing the spectra for $\vartheta = 30$ and 150° in the neutron energy region above 5 MeV, in view of the insufficient measurement accuracy.

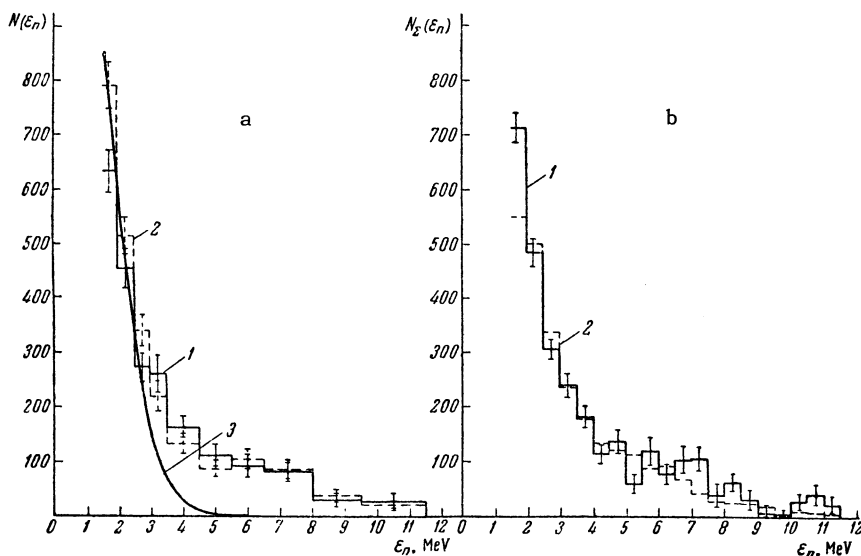


FIG. 9. a – energy distribution of photoneutrons from tantalum at $(h\nu)_{\max} = 19$ MeV; histogram 1 – $N_{90^\circ} + N_{270^\circ}$; 2 – $N_{30^\circ} + N_{150^\circ}$; curve 3 – spectrum of neutrons calculated in accordance with the evaporation model; b – summary neutron spectra for tantalum (1) and bismuth (2) for $(h\nu)_{\max} = 19$ MeV.

The spectrum obtained for the neutrons emitted at right angle to the x-ray beam direction coincides, within the limits of experimental error, with the spectrum measured for tantalum at an angle $\varphi = 90^\circ$ at $(h\nu)_{\max} = 20$ MeV, by Cortini et al, who used the same method^[15].

As for the other elements, the energy spectrum of the photoneutrons from tantalum has an anomalously large yield of high-energy neutrons, in disagreement with the form of the spectrum calculated from the statistical theory (curve 3). No sharp angular anisotropy was observed for tantalum, as in the case of bismuth. The direct emission of photoneutrons from tantalum was not considered using the independent particle model, since the computation scheme proposed by Wilkinson does not hold for strongly deformed nuclei.

Figure 9b shows for comparison the summary spectra of neutrons from tantalum and bismuth (for 30, 90, 150, and 270°). The data given for bismuth are taken only from that irradiation series in which tantalum was also irradiated. Histograms 1 and 2 are aligned in the energy interval 2–5 MeV. As can be seen from the figure, the yield of "direct" neutrons from tantalum is the same or somewhat larger than from bismuth. Comparison of these data yields for tantalum a ratio N_d/N_{ev} approximately equal to 20%.

Cavallaro et al^[16], who worked with $(h\nu)_{\max} = 30$ MeV, compared the energy spectra of the neutrons at 90° for gold and tantalum. The yield of neutrons with $\epsilon_n > 5$ MeV from gold is approximately half that from tantalum. These data are in full agreement with the results of the present work.

The work was done at the P. N. Lebedev Physics Institute of the U.S.S.R. Academy of Sciences, in collaboration with the staff members of the N. G. Chernyshevskii Saratov State University. N. Ya. Avdokushina, L. V. Baranova, and L. P. Bogatkina helped with the scanning of the emulsions, for which the authors express their deep gratitude.

¹ Ferrero, Hanson, Malvano, Tribuno, *Nuovo cimento* **4**, 418 (1956). R. G. Baker and K. G. McNeill, *Proc. Int. Conf. on Nuclear Structure*,

Univ. of Toronto Press, 1960, p. 740. G. C. Reinhardt and W. D. Whitehead, *Nucl. Phys.* **30**, 201 (1962).

² V. F. Weisskopf, *Statistical Theory of Nuclear Reactions*, (Russ. Transl.) IIL, 1952, p. 71.

³ B. I. Gavrilov and L. E. Lazareva, *JETP* **30**, 855 (1956), *Soviet Phys. JETP* **3**, 871 (1956).

⁴ L. J. Schiff, *Phys. Rev.* **70**, 87 (1946) and **83**, 252 (1950).

⁵ H. L. Poss, *Phys. Rev.* **79**, 539 (1959), G. A. Price, *Phys. Rev.* **93**, 1279 (1954). Ferrero, Hanson, Malvano, and Tribuno, *Nuovo cimento* **4**, 418 (1956). Zatsepina, Lazareva, and Pospelov, *JETP* **32**, 27 (1957), *Soviet Phys. JETP* **5**, 2 (1957). Emma, Milone, Rubbino, and Malvano, *Nuovo cimento* **17**, 365 (1960). Wataghin, Costa, Freire, and Goldenberg, *Nuovo cimento* **19**, 864 (1961).

⁶ J. Eichler and H. A. Weidenmuller, *Z. Physik* **152**, 261 (1958).

⁷ Ross, Mark, and Lawson, *Phys. Rev.* **102**, 1613 (1956).

⁸ D. Wilkinson, *Physica* **22**, 1039 (1956).

⁹ J. M. Blatt and V. F. Weisskopf, *Theoretical Nuclear Physics*, (Russ. Transl.) IIL, 1954, p. 285 [Wiley, N.Y., 1952].

¹⁰ M. Lax and H. Feshbach, *J. Acoust. Soc. Amer.* **20**, 108 (1948).

¹¹ P. E. Nemirovskii, *Yadernye reaktsii pri malykh i srednikh energiyakh* (Nuclear Reactions at Low and Medium Energies), AN SSSR 1958, p. 109.

¹² D. Wilkinson, *Proc. 1954 Glasgow Conf. on Nuclear Physics*, London-N.Y., 1955, p. 161.

E. D. Courant, *Phys. Rev.* **82**, 703 (1951).

¹³ Bertozzi, Paolini, and Sargent, *Phys. Rev.* **110**, 790 (1958).

¹⁴ M. Goeppert-Mayer and J. H. D. Jensen, *Elementary Theory of Nuclear Shell Structure*, Wiley, N.Y., 1955.

¹⁵ Cortini, Milone, Rubbino, and Ferrero, *Nuovo cimento* **9**, 85 (1958).

¹⁶ Cavallaro, Emma, Milone, and Rubbino, *Nuovo cimento* **9**, 736 (1958).

Translated by J. G. Adashko
283